PAN
ARCHIVES OF ACOUSTICS
Vol. **46**, No. 1, pp. 87–93 (2021)
DOI: 10.24425/aoa.2021.136563

Research Paper

Analysis of a Geometrical-Stiffening Membrane Acoustic Metamaterial with Individually Tunable Multi-Frequencies

Junjuan ZHAO[(1)*], Xianhui LI[(1)], David THOMPSON[(2)], Yueyue WANG[(1)], Wenjiang WANG[(1)], Liying ZHU[(1)], Yunan LIU[(1)]

[(1)] *Beijing Key Lab of Environmental Noise and Vibration*
Beijing Municipal Institute of Labor Protection
Beijing, China, 100054
*Corresponding Author e-mail: tianqi35@163.com

[(2)] *Institute of Sound and Vibration Research*
University of Southampton
Southampton, UK, SO171BJ

(*received July 29, 2020; accepted November 18, 2020*)

To realize a structure which can be conveniently tuned to multiple and wideband frequency ranges, a geometrical-stiffening membrane acoustic metamaterial (MAM) with individually tunable multiple frequencies is presented. The MAM is realized by a stacked arrangement of two membrane-magnet elements, each of which has a membrane with a small piece of steel attached in the centre. It can be tuned individually by adjusting the position of its compact magnet. The normal incidence sound transmission loss of the MAM is investigated in detail by measurements in an impedance tube. The test sample results demonstrate that this structure can easily achieve a transmission loss with two peaks which can be shifted individually in a wide low-frequency range. A theoretical consideration is analysed, the analysis shows that the magnetic effect related to this distance leads to a nonlinear attractive force and, consequently, nonlinear geometrical stiffening in each membrane-magnet element, which allows the peaks to be shifted. A reasonable design can make the structure have a good application prospect for low-frequency noise insulation where there is a need to adjust the transmission loss according to the spectrum of the noise source.

Keywords: membrane acoustic metamaterial; nonlinear geometric stiffening; low frequency tuning; sound transmission.

1. Introduction

During the last two decades, many researchers in physics and acoustical engineering have focused on acoustic metamaterials (Fang *et al.*, 2006; Lee *et al.*, 2009; Liang *et al.*, 2009; Zhang *et al.*, 2011; Mei *et al.*, 2012). Most membrane-type acoustic metamaterials (MAMs) once fabricated cannot adapt to real-life scenarios; they are passive and hardly adjustable, and their application is impractical in environments (Ding *et al.*, 2010; Fey *et al.*, 2011; Li *et al.*, 2004; Guenneau *et al.*, 2007; Lee *et al.*, 2010; Yang *et al.*, 2013). Then a substantially dynamic approach to mitigate these problems is an urgent matter to control low frequency noise. Chen *et al.* (2014a) applied a gradient magnetic field to actively tune the MAMs. This enables the shifting of the membrane eigenfrequencies during operation by selecting appropriate external magnetic field gradients. However, in the experiments, a large permanent magnet was used to generate the required magnetic field, which greatly increases the overall mass and size of this active MAM. A different realization of an active MAM was recently proposed by Xiao *et al.* (2015), who showed that the MAMs can be easily tuned by applying an external voltage, and used a setup similar to that of a condenser microphone with an acoustically transparent fishnet electrode and the added mass on the MAM acting as the counter electrode. By applying an external DC voltage, the eigen frequency of the MAM could be decreased due to the additional attractive force between the electrodes. This design requires the supply of a constant voltage

in every unit cell of the active MAM. For many potential fields of application, where a large surface needs to be covered with such active MAMs, considerable amounts of wiring are required to provide each unit cell with the suitable voltage, thus increasing the mass and installation effort of the active MAM structures. Furthermore, in some cases it might be infeasible to use electrical wirings inside noise protection devices due to safety regulations. Langfeldt *et al.* (2016) designed a new realization of an active MAM that employs a centralized actuation principle for adjusting the dynamic MAM properties without requiring individual electrical circuits in each MAM unit cell. This design requires that the materials of the membrane and the frame must be airtight so that the air volume between the MAMs and the frame can be pressurized using an external source of pressurized air connected to the MAMs via tubing or channels inside the frame. However, the fully sealed design lacks feasibility under some complex environments, and the slightest rupture of the membrane can cause the structure to lose its original purpose. Ma *et al.* (2018) achieved an actively reconfigurable acoustic metasurface that can play the crucial role of a deep-subwavelength, phase-modulating binary spatial sound modulator (SSM). This work mainly focused on the SSM's switchable property between two states through an electromagnet and did not pay much attention to the continuously tunable characteristics and frequency tuning range of the structure.

Efficient theoretical models to estimate the transmission loss of MAMs are demanded on account of the high potential of MAMs in low frequency sound insulation. For membranes loaded with a rigid mass, some of the first theoretical studies were carried out (Kornhauser *et al.*, 1953; Cohen *et al.*, 1957), in which the influence of a concentric circular mass on the natural frequencies of a circular membrane has been investigated. Further theoretically analyses for this case was done, the natural frequencies and mode shapes are given for the concentrically loaded circular membrane (Wang, 2003). Zhang *et al.* (2012) proposed an analytical model of a rectangular mass loaded a rectangular membrane specifically tailored for the application to MAMs, the forced vibration behaviour of membrane loaded with a mass was obtained by employing Galerkin method. Later, an analytical model for a circular membrane with a concentric ring mass was derived using the analogous approach (Tian *et al.*, 2013). However, the two models do not give reasons for the rigidity and rotary inertia of the masses. Therefore, Chen *et al.* (2014b) proposed a most comprehensive analytical model of MAMs recently. These theoretical methods are also suitable for tunable structures. An analytical model for the transmission loss calculation of thin rectangular and circular membranes loaded with adjustable acoustic properties has been presented by (Langfeldt *et al.*, 2016). These theoretical studies are of great help to our theoretical analysis.

Our preliminary work (Zhao *et al.*, 2019) presented a new approach can be tuned conveniently by adjusting its position using a screw. It is a single layer structure for limited low frequency sound isolation and can achieve only a single low-frequency transmission peak in a given state. To realize a structure which can be conveniently tuned to multiple and wideband frequency ranges, a new design of geometrical-stiffening membrane acoustic metamaterial is presented with individually tunable multiple frequencies. Theory, simulation and experiment methods are employed to study the normal incidence sound transmission loss of the MAM. The magnetic effect related to a nonlinear attractive force and, consequently, nonlinear geometric stiffening in each membrane-magnet element, which allows the peaks to be shifted, is analysed in this paper.

2. Structure

The basic structure of the geometrical-stiffening membrane acoustic metamaterial is shown in Fig. 1. The MAM is realized by a stacked arrangement of two membrane-magnet elements separated by an air gap and suspended from a support frame. Each element

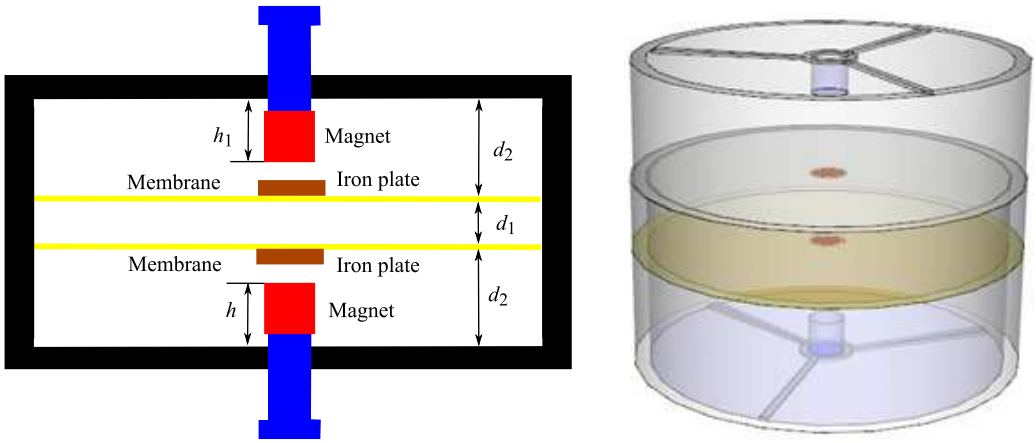

Fig. 1. Schematic of the geometrical-stiffening MAM.

has a membrane with a small iron platelet attached in the centre, a compact magnet and a solid ring support frame. The membrane has a radius $R = 50$ mm, thickness $d = 0.14$ mm and density $\rho = 1.329 \cdot 10^{-3}$ g/mm^3 and is fixed on a solid ring support frame. The iron platelet has radius $r = 5$ mm and mass $m_0 = 300$ mg. The solid ring support frame is a circular aluminium ring with an outer diameter of 100 mm, a thickness of 2.5 mm, a height of $d_2 = 15$ mm, designed to hold the membrane and fix the tuned central magnet at a certain distance from the platelet by a triangular structure. The magnet has radius 4 mm, top magnetic induction intensity 4830 Gs and its top height h can be tuned easily in a range 5 mm to 15 mm, so the distance to the platelet is between 10 mm and close to 0 mm, depending on the deformation of the membrane. The two elements of the unit cell are set symmetrically, combined with each other by the interval support frame which is also a circular aluminium ring with an outer diameter of 100 mm, a thickness of 2.5 mm, a height of $d_1 = 10$ mm. This is the maximum distance, verified by experiment (Zhao *et al.*, 2019), over which the magnet exerts a force on the iron platelet. This ensures that each magnet only has an effect on its own element. The heights of the two magnets, h and h_1 can be adjusted independently.

3. Theory analysis

The MAM is realized by a stacked arrangement of two membrane-magnet elements separated by an air gap and suspended from a support frame. Each magnet only has an effect on its own element. The first anti-resonance frequency prediction model for a single layer structure (one element) has been presented in preliminary work (Zhao *et al.*, 2019). This is also suitable for the geometrical-stiffening MAM to predict its isolation peaks in each element.

When an incident harmonic acoustic wave excited on the structure, the magnetic force exerted on the rigid iron platelet is (Zhao *et al.*, 2019):

$$F' = F + k_n \Delta x, \tag{1}$$

where F is the magnetic force which the magnet acted on the rigid iron platelet, Δx is the harmonic variation of the membrane, which is a small value introduced by F. There are two parts in Eq. (1): the constant force value F, and a force which dependent on k_n that relates to Δx. The freedom position of the iron mass is shifted by the first part F slightly, whereas an extra dynamic force on the platelet is the second term. The stiffness k_n can be calculated as:

$$k_n = \frac{\mathrm{d}F}{\mathrm{d}x} = \frac{2\phi}{(d_2 - h - x)^3} = \frac{2F}{l}, \tag{2}$$

where x is the iron platelet displacement from its freedom position due to the magnetic affect, the constant ϕ depends on the magnetic field, and $l = d_2 - h - x$ is the distance between the iron mass and the magnet top.

The first anti-resonance frequency of the one element could be described by,

$$f_a \approx \frac{\mu_{21}}{\mu_1} f_r = \frac{\mu_{21}}{\mu_1} \frac{1}{2\pi} \sqrt{\frac{k}{m}} = \frac{2.136}{2\pi} \sqrt{\frac{k_0 + k_n}{m}}, \tag{3}$$

where f_r is the first resonance mode can be expressed by a simple spring-mass model (Morse *et al.*, 1986), k is the total stiffness, comprised of k_0 which is determined by the membrane's pre-stress and k_n due to the magnet. The first anti-resonance mode without magnet, f_{a_0}, can be derived from experimental observations shown below in Fig. 5 as $f_{a0} = 148$ Hz from which k_0 can be estimated as $k_0 \approx m\left(\frac{2\pi}{2.136} f_{a0}\right)^2 \approx 315.8$ N/m according to a simple spring mass model and m is the combined mass of the membrane and iron platelet (1.669 g). μ_1 is the first root of the zero order Bessel function, μ_{21} is the first root of the second order Bessel function.

The static magnetic force F exerted on the rigid iron platelet was measured using a dynamometer as the distance l between the magnet top and the centralized rigid iron platelet (test point) varied, the magnetic force from test results and the stiffness obtained using Eq. (2) can be plotted, thus, the first anti-resonance frequencies of the element could also be calculated and predicted from Eq. (3), the results are as shown in Fig. 2. This simple theoretical analysis can quickly and accurately help us predict the peak frequency of trans-

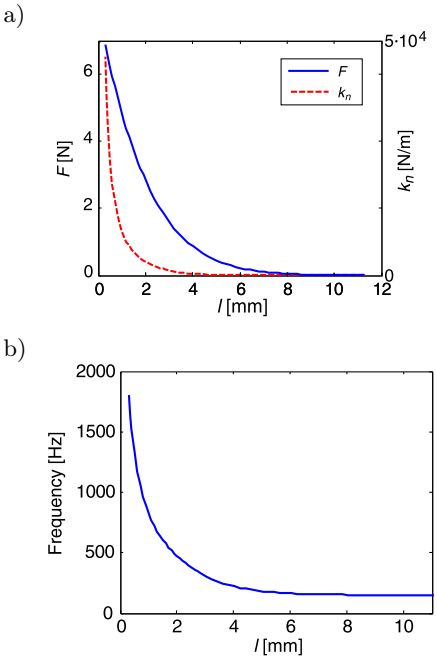

Fig. 2. a) Measured static magnetic force F exerted on the rigid iron platelet, and k_n obtained according to F; b) predicted first anti-resonance frequencies plotted against relative distance l.

mitting loss for the application structure design. The more complicated model to describe the membrane behavior (such as whole transmitting loss, phase information, etc.) will be developed in the following work.

4. Experiments and analysis

The normal incidence sound transmission loss of the MAM is investigated in detail by measurements in an impedance tube. The sound transmission loss is defined as: $TL(\omega) = 10\lg(W_i/W_t)$, where W_i and W_t are the airborne sound power incident on the sample and the sound power transmitted by the sample. It was measured under normal incidence using a Bruel & Kjaer Type 4206 large sample tube. The mathematical formulation is based on the transfer matrix representation, which has been widely used in the past both to analyze and to measure the acoustical properties of flow system elements, the theoretical base for this method of measurements has been better explained in the instruction manual of Bruel & Kjaer Type 4206. At one end, the tube features a loudspeaker providing broadband, stationary random excitation to the system. At the other end, the tube can be fitted with termination conditions. The internal volume of the tube is divided into two sections by a test sample under investigation, extending across the tube cross-section, as shown in Fig. 3. This type of sample tube shown in Fig. 4 has an inner diameter of 100 mm and is rated for a frequency range of 50–1600 Hz.

The transmission losses of the MAM in different conditions were tested. First, the transmission loss of the geometrical-stiffening MAM without magnets was tested, shown in Fig. 5, the value of f_{a0} is identified as 148 Hz. This is a key parameter to estimate the initial stiffness of the membrane with iron platelet of the geometrical-stiffening MAM.

Then, introducing the magnets, measured results are depicted in Fig. 6 in which the magnet top height h = 5 mm is kept constant in the first element, while the other magnet top heighth_1 in the second element is varied from 5 mm to 10.7 mm. The transmission loss peaks belonging to the first element with h = 5 mm are almost unchanged at the same frequency of about 150 Hz. This is the same frequency as found without

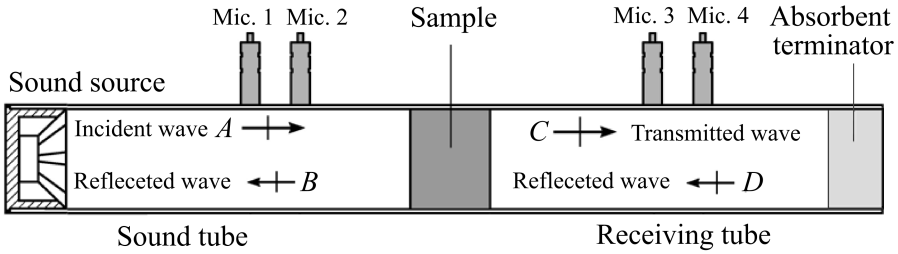

Fig. 3. Transmission Loss experimental setup.

Fig. 4. The Brüel and Kjær Transmission Loss Type 4206.

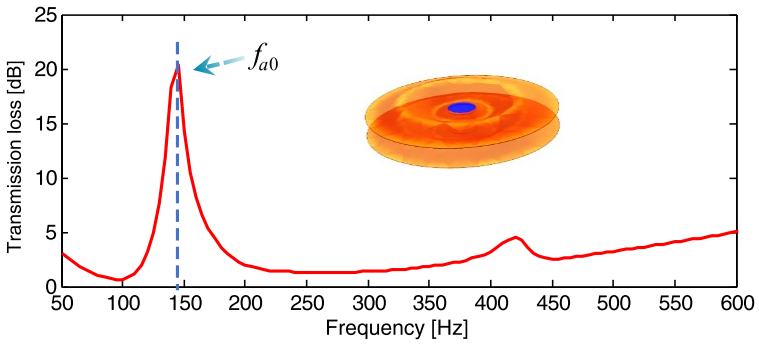

Fig. 5. Transmission loss of the geometrical-stiffening MAM without magnet.

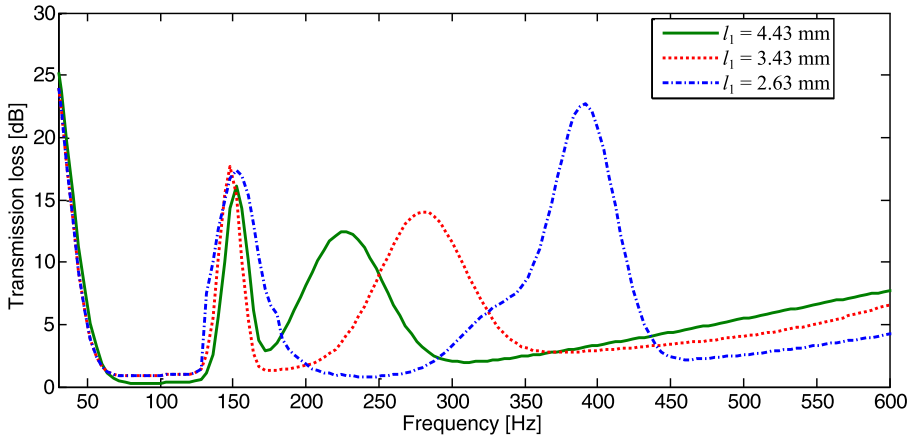

Fig. 6. Measured transmission losses of the MAM at different tuned conditions with h = 5 mm.

the magnet in Fig. 5 because the magnet is about 10 mm away from the platelet which is the distance where it has minimal effect. The transmission loss peaks in the curves due to the second element are seen to shift in a range about from 150 to 400 Hz as the magnet top height h_1 is increased from 5 mm to 10.7 mm while the distance l_1 decreased from 10 mm to 2.63 mm due to the nonlinear geometric stiffening in the element introduced by the magnetic force, in other words, the frequency increases when the magnet gets closer to the membrane because of the increased tension in the membrane.

After that, the magnet top height h_1 = 10.7 mm is kept constant in the second element, while the other magnet top height h in the first element is varied from 5 mm to 13.9 mm, and the distance l decreased from 10 mm to 1 mm, at which point it almost comes into contact with the iron platelet. These results are depicted in Fig. 7. The transmission loss peaks belonging to the second element with h = 10.7 mm are almost unchanged at the same frequency of about 360 Hz. The transmission loss peaks in the curves due to the first element are seen to shift in a wide range from about 150 to 800 Hz as the magnet top height h is increased from 5 mm to 13.9 mm. The two elements can also be tuned at the same time to suit any frequency required for noise control.

The experiment and theory predicted results of the transmission loss peaks for the two elements of the MAM can be plotted in Fig. 8, which indicates that the experimental transmission loss peaks for each ele-

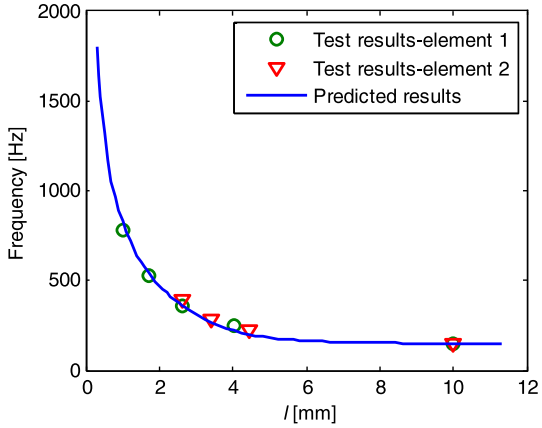

Fig. 8. The relationship between the transmission loss peak and distance l in element.

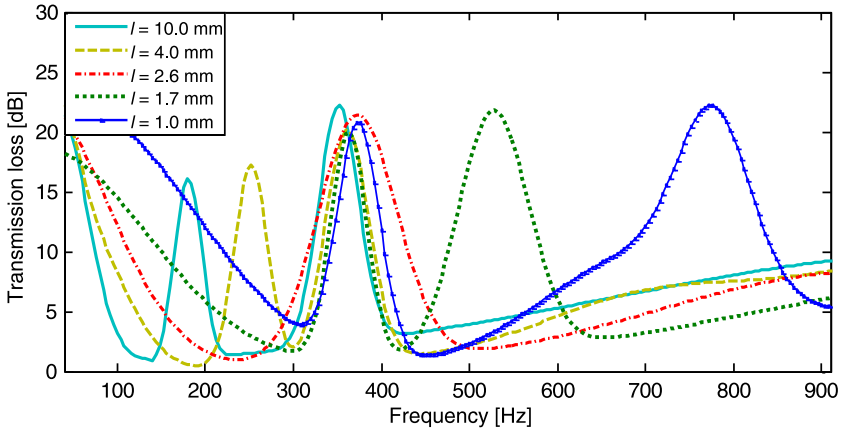

Fig. 7. Measured transmission losses of the MAM at different tuned conditions with h_1 = 10.7 mm.

ments of the MAM derived from the impedance tube measurements are in good agreement with those predicted theoretically. The relationships between the transmission loss peaks and the distances in the elements tell us more explicitly how the tuned magnet top height as well as the distance l change the peaks. It is more helpful to judge the transmission loss peak frequency through the determination of the magnet position, it is very useful for our active control structure design in the future.

This design can thus easily and feasibly achieve two transmission loss peaks that are individually and flexibly tuneable over a very wide low-frequency range. From the analysis, it is shown that the position of the transmission loss peaks can be determined by adjusting the magnet top heights $h$or the distance l. The magnetic effect related to this distance leads to a nonlinear attractive force and, consequently, nonlinear geometric stiffening in each membrane-magnet element, which allows the peaks to be shifted. A reasonable design of membrane-magnet distance in each element can easily be used to realize individually-tuned multiple transmission loss peaks which make the structure have a good application prospect for low-frequency noise insulation where there is a need to adjust the transmission loss according to the spectrum of the noise source.

However, from the view of practical application, the applied conditions for this MAM need to be considered, especially for the magnet in the structure. The magnet used here is NdFeB magnet, it has an axial magnetic field, and its magnetic induction intensity on the top or bottom surface is 4830 Gauss. The magnet is permanent theoretically, if the environment where it is used meets some requirements, such as, the ambient temperature does not exceed 80°, and there are not any other high magnetic fields. Therefore, compared with other tunable structures (Xiao *et al.*, 2015; Langfeldt *et al.*, 2016; Ma *et al.*, 2018), the design cannot be applied in the environment that has high temperature and magnet field. In fact, for practical applications, this magnet can work for at least six years without weaken in environments that meet the requirements for permanent magnets, according to the tested results of magnets purchased six years ago in the lab. It may last longer, this will take time to verify, we will continue to pay attention to this issue in the future.

5. Conclusions

This paper demonstrates that a geometrical-stiffening membrane acoustic metamaterial can be realized to achieve high transmission loss at multiple low frequencies which are adjustable in a large frequency range; the peaks can be easily tuned individually by applying small magnets, the top height of which can be tuned conveniently. The acoustical properties of the design are investigated through theory analysis and experiments. These showed that the geometrical-stiffening MAM with two elements can be tuned easily and feasibly at the same time to suit any frequency at which control is required in a wide range from about 100 to 800 Hz. The tuning is achieved due to the regime of the nonlinear geometric stiffening introduced by the adjustable magnet top height in the design. The results demonstrate that a reasonable design of membrane-magnet distance in each element can easily be used to realize individually-tuned multiple transmission loss peaks which make the structure have a good application prospect for low-frequency noise insulation where there is a need to adjust the transmission loss according to the spectrum of the noise source.

Acknowledgements

This work is supported by the National Natural Science Foundation of China (No. 11704035); China State Scholarship Fund (No.201909110048); Beijing Nova Program (No. Z181100006218018); Beijing Natural Science Foundation (No. 1202008, 3204041); Beijing excellent talent project-top individual; Beike Scholar Project (BS201901); Beijing Postdoctoral Research Foundation; Xicheng District excellent talent project (No. 20180029).

References

1. Chen X., Xu X., Ai S., Chen H., Pei Y., Zhou X. (2014a), Active acoustic metamaterials with tunable effective mass density by gradient magnetic fields, *Applied Physics Letters*, **105**(7): 071913, doi: 10.1063/1.4893921.

2. Chen Y., Huang G., Zhou X., Hu G., Sun C.T. (2014b), Analytical coupled vibroacoustic modeling of membrane-type acoustic metamaterials: Membrane model, *Journal of the Acoustical Society of America*, **136**(3): 969–979, doi: 10.1121/1.4892870.

3. Cohen H., Handelman G. (1957), On the vibration of a circular membrane with added mass, *Journal of the Acoustical Society of America*, **29**(2): 229–233, doi: 10.1121/1.1908838.

4. Ding C., Hao L., Zhao X. (2010), Two-dimensional acoustic metamaterial with negative modulus, *Journal of Applied Physics*, **108**(7): 074911, doi: 10.1063/1.3493155.

5. Fang N. *et al.* (2006), Ultrasonic metamaterials with negative modulus, *Nature Materials*, **5**(6): 452–456, doi: 10.1038/nmat1644.

6. Fey J., Robertson W.M. (2011), Compact acoustic bandgap material based on a subwave length collection of detuned Helmholtz resonators, *Journal of Applied Physics*, **109**(11): 114903, doi: 10.1063/1.3595677.

7. Guenneau S., Movchan A., Pétursson G., Ramakrishna S.A. (2007), Acoustic metamaterials for sound focusing and confinement, *New Journal of Physics*, **9**(11): 399, doi: 10.1088/1367-2630/9/11/399.

8. Kornhauser E.T., Mintzer D. (1953), On the vibration of mass-loaded membranes, *Journal of the Acoustical Society of America*, **25**(5): 903–906, doi: 10.1121/1.1907216.

9. Langfeldt F., Riecken J., Gleine W., Von Estorff O. (2016), A membrane-type acoustic metamaterial with adjustable acoustic properties, *Journal of Sound & Vibration*, **373**: 1–18, doi: 10.1016/ j.jsv.2016.03.025.

10. Lee S.H., Park C.M., Seo Y.M., Wang Z.G., Kim C.K. (2009), Acoustic metamaterial with negative modulus, *Journal of Physics: Condensed Matter*, **21**(17): 175704, doi: 10.1088/0953-8984/21/17/ 175704.

11. Lee S.H., Park C.M., Seo Y.M., Wang Z.G., Kim C.K. (2010), Composite acoustic medium with simultaneously negative density and modulus, *Physical Review Letters*, **104**(5): 054301, doi: 10.1103/PhysRevLett.104.054301.

12. Li J., Chan C.T. (2004), Double-negative acoustic metamaterial, *Physical Review E*, **70**: 055602, doi: 10.1103/PhysRevE.70.055602.

13. Liang B., Yuan B., Cheng J.C. (2009), Acoustic diode: rectification of acoustic energy flux in one-dimensional systems, *Physical Review Letters*, **103**(10): 104301, doi: 10.1103/PhysRevLett.103.104301.

14. Ma G., Fan X., Sheng P., Fink M. (2018), Shaping reverberating sound fields with an actively tunable metasurface, *Proceedings of the National Academy of Sciences*, **115**(26): 6638–6643, doi: 10.1073/pnas. 1801175115.

15. Mei J., Ma G., Yang M., Yang Z., Wen W., Sheng P. (2012), Dark acoustic metamaterials as super absorbers for low-frequency sound, *Nature Communications*, **3**(27): 7561–7567, doi: 10.1038/NCOMMS1758.

16. Morse P.M., Ingard K.U. (1986), *Theoretical Acoustics*, Princeton University Press, pp. 209–213.

17. Tian H., Wang X., Zhou Y. (2013), Theoretical model and analytical approach for a circular membrane-ring structure of locally resonant acoustic metamaterial, *Applied Physics A*, **114**(3): 985–990, doi: 10.1007/ s00339-013-8047-y.

18. Wang C.Y. (2003), Vibration of an annular membrane attached to a free, rigid core, *Journal of Sound and Vibration*, **260**(4): 776–782, doi: 10.1016/S0022-460X(02)01198-7.

19. Xiao S., Ma G., Li Y., Yang Z., Sheng P. (2015), Active control of membrane-type acoustic metamaterial by electric field, *Applied Physics Letters*, **106**(9): 091904, doi: 10.1063/1.4913999.

20. Yang M., Ma G., Yang Z., Sheng P. (2013), Coupled membranes with doubly negative mass density and bulk modulus, *Physical Review Letters*, **110**(13): 134301, doi: 10.1103/PhysRevLett.110.134301.

21. Zhang S., Xia C., Fang N. (2011), Broadband acoustic cloak for ultrasound waves, *Physical Review Letters*, **106**(2): 024301, doi: 10.1103/PhysRevLett.106.024301.

22. Zhang Y., Wen J., Xiao Y., Wen X., Wang J. (2012), Theoretical investigation of the sound attenuation of membrane-type acoustic metamaterials, *Physics Letters A*, **376**(17): 1489–1494, doi: 10.1016/j.physleta.2012.03.010.

23. Zhao J., Li X., Wang W., Wang Y., Zhu L., Liu Y. (2019), Membrane-type acoustic metamaterials with tunable frequency by a compact magnet, *Journal of the Acoustical Society of America*, **145**(5): EL400–EL404, doi: 10.1121/1.5107431.